Efficient Electromagnetic Modeling of Three-Dimensional Multilayer Microstrip Antennas and Circuits

Feng Ling, *Member, IEEE*, Jian Liu, *Student Member, IEEE*, and Jian-Ming Jin, *Fellow, IEEE*

***Abstract*—An efficient method-of-moments (MoM) solution is presented for analysis of multilayer microstrip antennas and circuits. The required multilayer Green's functions are evaluated by the discrete complex image method (DCIM), with the guided-mode contribution extracted recursively using a multilevel contour integral in the complex k_ρ-plane. An interpolation scheme is employed to further reduce the computer time for calculating the Green's functions in the three-dimensional (3-D) space. Higher order interpolatory basis functions defined on curvilinear triangular patches are used to provide necessary flexibility and accuracy for the discretization of arbitrary shapes and to offer a better convergence than lower order basis functions. The combination of the improved DCIM and the higher order basis functions results in an efficient and accurate MoM analysis for 3-D multilayer microstrip structures.**

***Index Terms*—Green's function, higher order method, method of moments, microstrip antennas, microstrip circuits, numerical analysis.**

I. INTRODUCTION

THE method-of-moments (MoM) solution of integral equations has received intense attention to tackle the multilayer medium problems. In this method, the evaluation of Green's functions and the choice of basis functions are crucial to obtaining an accurate and efficient solution.

The Green's function for multilayered media has the form of a Sommerfeld integral. In general, the analytical solution of this integral is not available, and the numerical integration is time consuming since the integrand is both highly oscillating and slowly decaying. Several efficient techniques have been proposed to speed up this numerical integration [1]. Recent efforts to further accelerate the computation include the fast Hankel transform (FHT) approach [2], [3], the steepest descent path (SDP) approach [4], the window function approach [5], and the discrete complex image method (DCIM) [6]–[16].

In this paper, an improved DCIM is employed to efficiently evaluate the Green's functions. The spectral-domain Green's functions for multilayer media are first derived from a simple transmission-line perspective. The DCIM is then employed to efficiently evaluate the Sommerfeld integrals, resulting in closed-form spatial-domain Green's functions. To evaluate the far-field Green's functions accurately, it is necessary to extract surface waves to approximate $1/\sqrt{\rho}$ asymptotic behavior. In the previous research on the DCIM, the surface-wave contribution is treated analytically by using residue calculus, which makes it difficult to be extended to multilayer cases. Here, the surface-wave contribution is obtained by performing a contour integral recursively in the complex k_ρ-plane [16]. This approach works for a general multilayer medium with an arbitrary number of layers, whether open or shielded and lossy or lossless. To make the Green's function evaluation even more efficient, especially for three-dimensional (3-D) structures, an interpolation scheme is employed, which is able to recompute the Green's functions as efficiently as in free-space problems.

The choice of basis functions is also critical for the MoM analysis. Traditional numerical modeling employs rooftop functions for rectangular elements or Rao–Wilton–Glisson (RWG) functions [17] for triangular elements. These functions are complete to the zeroth order in a sense that they have constant normal and linear tangential components at element edges and their divergence, which represents the charge density, is a constant within each element. As a result, a very fine discretization is often required to yield an accurate solution. This leads to a large matrix equation, which is expensive to solve. In addition, the numerical solution converges slowly to the exact one when the discretization is made finer. As a solution to this problem, higher order basis functions have been developed [18]–[20]. In this study, the higher order interpolatory basis functions defined on curvilinear triangular patches [19] are employed, which have a better convergence rate and can yield an accurate solution with a rather coarse discretization. Combining the higher order basis functions with the DCIM yields an efficient and accurate MoM analysis for 3-D multilayer microstrip structures.

Manuscript received February 22, 2000; revised July 26, 2001. This work was supported by the Air Force Office of Scientific Research under a grant from the Multidisciplinary University Research Initiative Program under Contract F49620-96-1-0025, and by the National Science Foundation under Grant NSF ECE 94-57 735.

F. Ling was with the Center for Computational Electromagnetics, Department of Electrical and Computer Engineering, University of Illinois at Urbana-Champaign, Urbana, IL 61801-2991 USA. He is now with the Semiconductor Products Sector, Motorola, Tempe, AZ 85284 USA.

J. Liu and J.-M. Jin are with the Center for Computational Electromagnetics, Department of Electrical and Computer Engineering, University of Illinois at Urbana-Champaign, Urbana, IL 61801-2991 USA (e-mail: j-jin1@uiuc.edu).

Publisher Item Identifier S 0018-9480(02)05213-4.

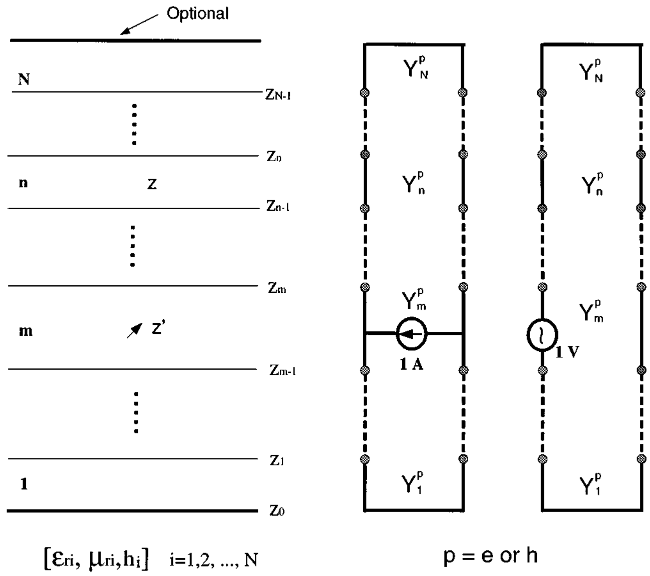

Fig. 1. Multilayer medium with source and field points in layer m and layer n, respectively, and its transmission-line representation.

II. Formulation

This section describes the evaluation of multilayer Green's functions using the improved DCIM and MoM solution using higher order basis functions.

A. Multilayer Medium Green's Functions

Consider a current source in a multilayer medium. Each layer is characterized by relative permittivity ϵ_r, relative permeability μ_r, and thickness h, as shown in Fig. 1. The electric field due to the current can be expressed in a mixed-potential form as

$$\mathbf{E} = -j\omega\mu_0 \langle \bar{\mathbf{G}}^A ; \mathbf{J} \rangle + \frac{1}{j\omega\epsilon_0} \nabla \langle G^\Phi, \nabla' \cdot \mathbf{J} \rangle \tag{1}$$

where $\mathbf{J}$ denotes the electric current density of the source, and $\bar{\mathbf{G}}^A$ and G^Φ are the Green's functions for the vector and scalar potentials, respectively. The detailed discussion in [21] shows that it is preferable to choose $\bar{\mathbf{G}}^A$ as

$$\bar{\mathbf{G}}^A = \begin{bmatrix} G_{xx}^A & 0 & G_{xz}^A \\ 0 & G_{xx}^A & G_{yz}^A \\ G_{zx}^A & G_{zy}^A & G_{zz}^A \end{bmatrix} \tag{2}$$

and G^Φ as the scalar potential for a horizontal electric dipole (HED).

In general, the Green's function for a multilayer medium is expressed in terms of a Sommerfeld integral, which can be written as

$$G(\boldsymbol{\rho}, z \,|\, z') = \frac{1}{2\pi} \int_0^\infty \tilde{G}(k_\rho, z \,|\, z') J_0(k_\rho \rho) k_\rho dk_\rho \tag{3}$$

where $\tilde{G}$ is the spectral-domain counterpart of G. The derivation of the spectral-domain Green's functions for multilayer media can be accomplished by constructing equivalent transmission lines [21], [22]. The original problem to find electric and magnetic fields is thus converted to the problem of obtaining the voltages and currents of the corresponding transmission lines. From the voltages and currents, the Green's functions for the vector potential $\tilde{\tilde{\mathbf{G}}}^A$ and the scalar potential $\tilde{G}^\Phi$ can be derived as

$$\tilde{G}_{xx}^A = \frac{1}{j\omega\mu_0} V_i^h \tag{4}$$

$$\tilde{G}_{zt}^A = \frac{\mu_r k_t}{j k_\rho^2} \left(I_i^h - I_i^e \right), \qquad t = x, y \tag{5}$$

$$\tilde{G}_{zz}^A = \frac{1}{j\omega\epsilon_0} \left[\left(\frac{\mu_r}{\epsilon_r'} - \frac{\mu_r' k_z^2}{\epsilon_r k_\rho^2} \right) I_v^e + \frac{k_0^2 \mu_r \mu_r'}{k_\rho^2} I_v^h \right] \tag{6}$$

$$\tilde{G}^\Phi = \frac{j\omega\epsilon_0}{k_\rho^2} \left(V_i^e - V_i^h \right) \tag{7}$$

where $V_i^{e,h}$ and $I_i^{e,h}$ are the voltages and currents of the equivalent transmission line. $\tilde{G}_{xz}^A$ and $\tilde{G}_{yz}^A$ are related to $\tilde{G}_{zx}^A$ and $\tilde{G}_{zy}^A$ by the reciprocity principle, which gives

$$\tilde{G}_{tz}^A(z \,|\, z') = -\frac{\mu_r'}{\mu_r} \tilde{G}_{zt}^A(z' \,|\, z). \tag{8}$$

Therefore, the Green's functions required in this method are $G_{xx}^A, G_{zz}^A, G_{zx}^A, G_{zy}^A$, and G^Φ. Furthermore, G_{zx}^A and G_{zy}^A have the same kernels so that a total of only four Green's functions are required for evaluation.

Once the spectral-domain Green's functions are obtained, the DCIM can be applied to rapidly evaluate the Sommerfeld integrals. Rewrite the spectral-domain Green's function in a simple form as $\tilde{G} = AF/(2jk_{zm})$, where A is a constant. As the first step of the DCIM, the primary field term F_{pr} (which is the field in the absence of the multilayer medium) is extracted from F when the source and observation points are in the same layer. Note that there is no primary field term in $\tilde{G}_{zt}^A$. The static contributions F_{st}, which dominate as $k_\rho \to \infty$, are also extracted, making the remaining kernel decay to zero for a sufficiently large k_ρ. This happens only when both the source and field points are on an interface between two different layers. The next step is to extract the guided-mode contributions, denoted by F_{gm}. Here, the guided modes refer to surface-wave modes for open multilayer media, and both surface-wave modes and ground-plane guided modes for shielded multilayer media. In the previous DCIM, the guided-mode contributions are extracted analytically using residue calculus, which makes the DCIM difficult to be extended to multilayer media. As a result, to use the DCIM for multilayer media, the guided modes are often not extracted. However, the lack of the guided-mode extraction results in errors in the far-field region since the guided modes have $1/\sqrt{\rho}$ asymptotic behavior. For a general-purpose algorithm, especially for the MoM analysis of electrically large structures, the guided modes have to be extracted. In this study, the extraction of guided modes is carried out numerically by evaluating a contour integral in the complex k_ρ-plane [16]. It begins with the evaluation of the contour integral along a rectangle in the k_ρ-plane and a check of the computed value. If it is nonzero, the rectangle is subdivided into four sub-rectangles and the contour integral is performed on each of them. The process is repeated until the pole locations and residues are precisely determined. This multilevel method is very fast since it requires only $\log n$ steps to locate a pole with the precision of n digits.

	ε_r	h
3	1.0	9.238
2	2.2	0.254
1	10.2	0.508

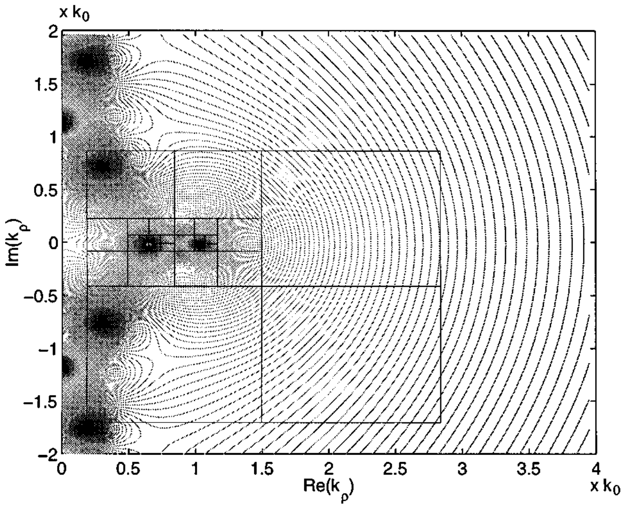

Fig. 2. Magnitude of $\tilde{G}^{\Phi}$ in the first and fourth quadrants of the complex k_ρ-plane for a shield three-layer medium at 20 GHz. Unit for thickness is millimeters.

To illustrate the process described above, a shielded three-layer medium [3] is considered. The magnitude of $\tilde{G}^{\Phi}$ in the first and fourth quadrants is plotted in Fig. 2 for the case that both the source and observation points are at the interface between the second and third layers and the frequency is at $f = 20$ GHz. The contour integral is repeated until we find the poles at $k_\rho = 0.671k_0, 0.719k_0$, and $1.055k_0$. The pole at $k_\rho = 1.055k_0$ corresponds to a surface wave. The other two poles are associated with the modes guided by the two ground planes. The poles on the imaginary axis corresponds to evanescent modes, which are not extracted in this method. If one of the ground planes is removed, the ground-plane guided modes become the continuous modes, or the radiation modes, which comprise the Sommerfeld branch cut [23]. The radiation modes are not extracted in this method.

After the guided-mode extraction, the generalized pencil-of-function (GPOF) method [24] is applied to approximate the remaining kernel. With the aid of the Sommerfeld identity, we can obtain the closed-form Green's functions for vector and scalar potentials.

However, the guided-mode extraction gives rise to a problem in the near-field calculation. It is well known that when $z \neq z'$, the Green's function is not singular at $\rho = 0$; however, the guided-mode term carries the singularity. To overcome this difficulty, a transition point is introduced to divide the near- and far-field regions. The DCIM is then applied twice, one with and the other without the guided-mode extraction [6], [13], [15]. The first calculates the Green's function for the near-field region, and the second calculates the Green's function for the far-field region. Fig. 3 shows the magnitudes of the four Green's functions $G_{xx}^A, G_{zx}^A, G_{zz}^A$, and G^{Φ} for the shielded three-layer medium depicted in Fig. 2. Fig. 4 displays the magnitudes of

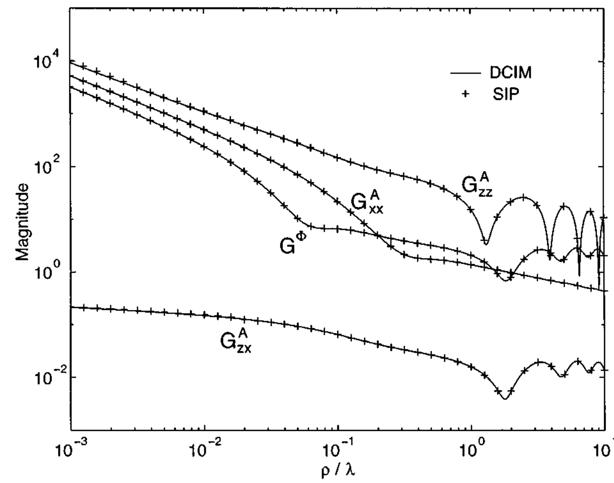

Fig. 3. Magnitude of Green's functions ($G_{xx}^A, G_{zx}^A, G_{zz}^A$, and G^{Φ}) for a shielded three-layer medium at 20 GHz with $z = z' = 0.762$ mm.

	ε_r	h
5	1.0	∞
4	2.1	0.7
3	12.5	0.3
2	9.8	0.5
1	8.6	0.3

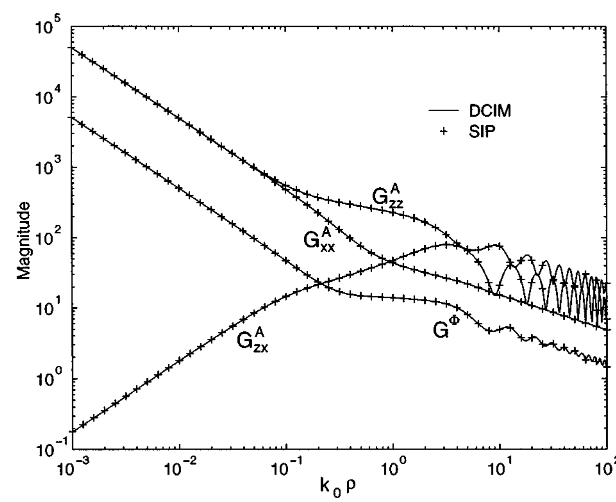

Fig. 4. Magnitude of Green's functions ($G_{xx}^A, G_{zx}^A, G_{zz}^A$, and G^{Φ}) for a five-layer medium at 30 GHz with $z = z' = 0.4$ mm. Unit for thickness is millimeters.

the Green's functions for a five-layer medium without a shield at the top. In both figures, the DCIM results are calculated using six complex images and compared with those obtained by direct numerical integration along the Sommerfeld integration path (SIP). The agreement in all cases is excellent.

The DCIM provides an efficient way to evaluate the Green's functions; however, issues about computer time still have to be considered since the number of Green's functions to be evaluated is proportional to $O(N^2)$ in the MoM analysis, where N denotes the number of unknowns. Since the guided modes

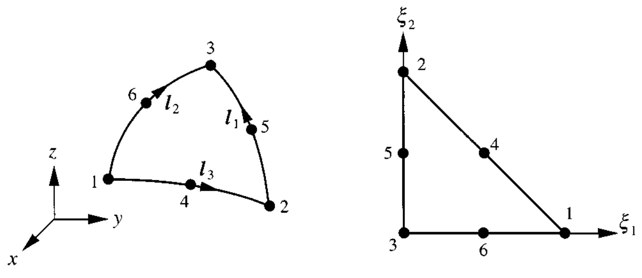

Fig. 5. (a) Curvilinear patch in the (x, y, z) space. (b) Transformed patch in the (ξ_1, ξ_2) plane.

are expressed in terms of the Hankel function, their evaluation is expensive compared to the evaluation of the remaining part. Furthermore, for structures supporting vertical currents, the Green's functions for all the different combinations of z and z' are needed. The DCIM has to be performed for every combination, although it is possible for some cases to generate the complex images that are independent of z and z'. To circumvent these problems, an interpolation scheme is usually employed [2], [14], [25]–[27]. In this scheme, sections along the z-axis where the structure is located are first determined, and then subdivided into N_s sheets. Hence, there are a total of N_s^2 combinations of z and z'. For each pair of sheets, the DCIM is performed and the Chebyshev interpolation is applied to the variable ρ [28]. For G_{xx}^A, G_{zz}^A, and G^Φ, the reciprocity principle can reduce the number of times to perform the DCIM to $N_s(N_s+1)/2$. When z and z' are located between those sheets, the Lagrange polynomial interpolation is employed for the variables z and z' [28].

With the interpolation strategy, the computer time to evaluate the Green's functions for multilayer media is further reduced in the MoM analysis. Moreover, it is possible to store the interpolation coefficients as a database instead of performing the interpolations online. Therefore, the generation of Green's functions can be decoupled from specific circuit geometries.

B. Higher Order Basis Functions

With an applied field $\mathbf{E}^a$, the induced current on microstrips can be found by solving the following mixed-potential integral equation (MPIE):

$$\hat{n} \times \left[-j\omega\mu_0 \langle \bar{\mathbf{G}}^A(\mathbf{r}, \mathbf{r}'); \mathbf{J}(\mathbf{r}') \rangle + \frac{1}{j\omega\epsilon_0} \nabla \langle G^\Phi(\mathbf{r}, \mathbf{r}'), \nabla' \cdot \mathbf{J}(\mathbf{r}') \rangle \right] = -\hat{n} \times \mathbf{E}^a(\mathbf{r}) \quad (9)$$

where $\hat{n}$ denotes the unit normal. To solve this integral equation by the MoM, the microstrip surface is first divided into curvilinear triangular patches, which offer more flexibility and accuracy to model arbitrary shapes than flat triangular patches with straight edges. A quadratic triangular patch is shown in Fig. 5(a), which is described by six nodes. After the coordinate transformation, shown in Fig. 5(b), we can easily describe any vector $\mathbf{r}$ on the patch in terms of the quadratic shape function φ_i

$$\mathbf{r} = \sum_{i=1}^{6} \varphi_i(\xi_1, \xi_2, \xi_3)\mathbf{r}_i \quad (10)$$

where the coordinates ξ_1, ξ_2, ξ_3 have the dependence relation as $\xi_1 + \xi_2 + \xi_3 = 1$ and the shape functions are given by

$$\begin{aligned} \varphi_1 &= \xi_1(2\xi_1 - 1) \\ \varphi_2 &= \xi_2(2\xi_2 - 1) \\ \varphi_3 &= \xi_3(2\xi_3 - 1) \\ \varphi_4 &= 4\xi_1\xi_2 \\ \varphi_5 &= 4\xi_2\xi_3 \\ \varphi_6 &= 4\xi_3\xi_1. \end{aligned} \quad (11)$$

The edge vectors can be calculated as

$$\boldsymbol{\ell}_1 = -\frac{\partial \mathbf{r}}{\partial \xi_2} \quad \boldsymbol{\ell}_2 = -\frac{\partial \mathbf{r}}{\partial \xi_1} \quad \boldsymbol{\ell}_3 = \frac{\partial \mathbf{r}}{\partial \xi_2} - \frac{\partial \mathbf{r}}{\partial \xi_1} \quad (12)$$

and the gradient vectors are evaluated by

$$\begin{aligned} \nabla\xi_1 &= \frac{\hat{n} \times \boldsymbol{\ell}_1}{\mathcal{J}} \\ \nabla\xi_2 &= \frac{\hat{n} \times \boldsymbol{\ell}_2}{\mathcal{J}} \\ \nabla\xi_3 &= -\nabla\xi_1 - \nabla\xi_2 \end{aligned} \quad (13)$$

where $\mathcal{J}$ is the Jacobian of the transformation.

The building blocks of the higher order interpolatory basis functions are the zeroth-order basis functions, which are given by

$$\mathbf{\Lambda}_\beta(\mathbf{r}) = \frac{1}{\mathcal{J}} \left(\xi_{\beta+1}\boldsymbol{\ell}_{\beta-1} - \xi_{\beta-1}\boldsymbol{\ell}_{\beta+1} \right), \qquad \beta = 1, 2, 3. \quad (14)$$

The zeroth-order basis functions on the flat triangular patch are also known as the RWG basis functions [17].

The higher order interpolatory vector basis functions on a given triangular patch are constructed by multiplying the zeroth-order basis functions with a set of polynomial functions [19]

$$\mathbf{\Lambda}_{ijk}^\beta(\mathbf{r}) = N_\beta \frac{(p+2)\xi_\beta \hat{\alpha}_{ijk}(\boldsymbol{\xi})}{i_\beta} \mathbf{\Lambda}_\beta(\mathbf{r}) \quad (15)$$

where β denotes the edge number associated with the zeroth-order basis function, i, j, and k are the indexes for labeling the interpolation points, which satisfy $i + j + k = p + 2$, and i_β takes i, j, or k for $\beta = 1, 2$, or 3, respectively. The normalization coefficients N_β are given by

$$N_\beta = \frac{p+2}{p+2-i_\beta} \ell_\beta. \quad (16)$$

The $\hat{\alpha}_{ijk}(\boldsymbol{\xi})$ is the polynomial function defined as

$$\hat{\alpha}_{ijk}(\boldsymbol{\xi}) = \hat{R}_i(p+2, \xi_1)\hat{R}_j(p+2, \xi_2)\hat{R}_k(p+2, \xi_3) \quad (17)$$

where the shifted Silvester–Lagrange polynomial $\hat{R}_i$ is given by

$$\hat{R}_i(p, \xi) = \begin{cases} \dfrac{1}{(i-1)!} \displaystyle\prod_{k=1}^{i-1} (p\xi - k), & 2 \le i \le p+1 \\ 1, & i = 1. \end{cases} \quad (18)$$

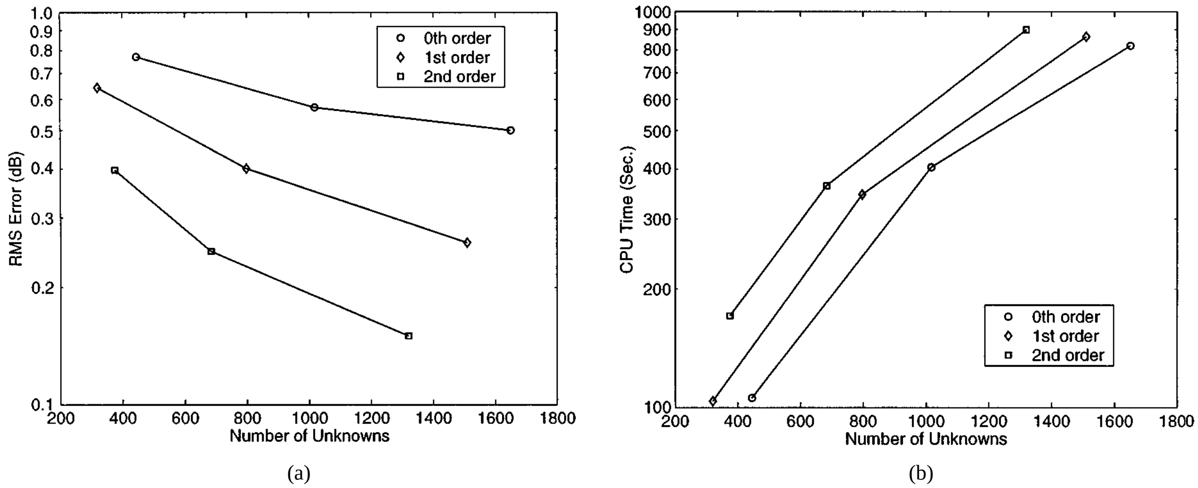

Fig. 6. Convergence behavior of the higher order basis functions (The reference solution is obtained using the third-order basis functions with an overly dense mesh). (a) rms error versus number of unknowns. (b) CPU time versus number of unknowns.

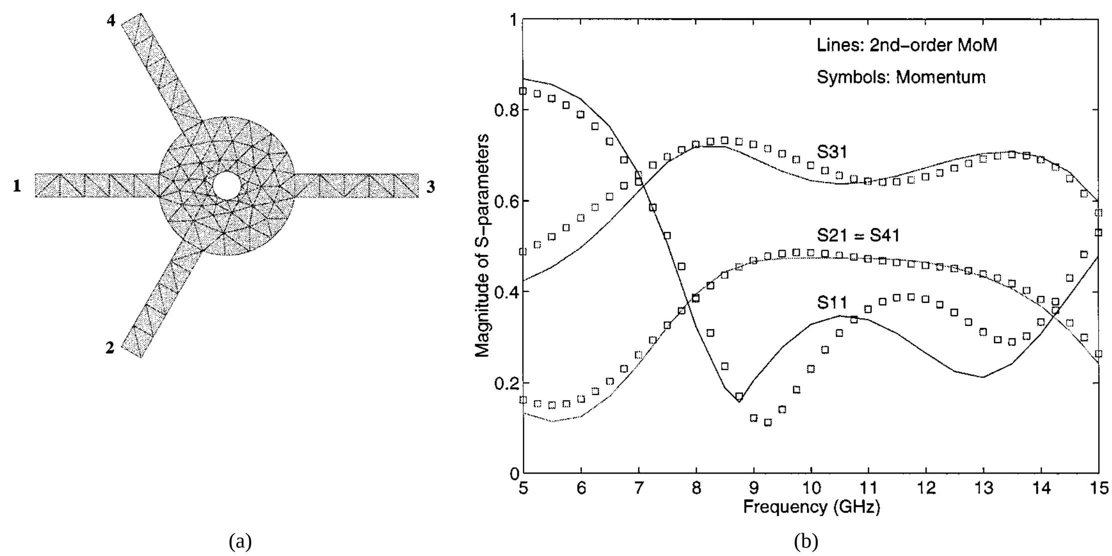

Fig. 7. S-parameters of an annular-ring microstrip power divider. The substrate has $\epsilon_r = 2.2$ and $h = 0.79$ mm. The linewidth is 2.4 mm. The inner and outer radii of the annular ring are 1.5 and 7.2 mm, respectively. The angles between ports 1 and 2 and ports 1 and 4 are 60°.

The number of degrees of freedom is $N_e = (p+1)(p+3)$ on a triangular patch for the basis functions of order p.

With the higher order basis functions described above, the current density on each patch can be expanded as

$$\mathbf{J}(\mathbf{r}) = \sum_{i=1}^{N_e} I_i \mathbf{\Lambda}_i(\mathbf{r}). \tag{19}$$

Substituting (19) into (9) and applying Galerkin's procedure, we obtain a matrix equation

$$\bar{\mathbf{Z}} \cdot \mathbf{I} = \mathbf{V} \tag{20}$$

where the global impedance matrix $\bar{\mathbf{Z}}$ and the right-hand-side vector are assembled from the local impedance matrix and local right-hand-side vector, respectively. For example, the local impedance matrix for patch m and patch n has the dimension $N_e \times N_e$, and the local right-hand-side vector has the dimension N_e, whose elements Z_{ij} and V_i are given by

$$Z_{ij}^{mn} = -j\omega\mu_0 \left\langle \mathbf{\Lambda}_i; \left\langle \bar{\mathbf{G}}^A; \mathbf{\Lambda}_j \right\rangle_{S_n} \right\rangle_{S_m} - \frac{1}{j\omega\epsilon_0} \left\langle \nabla \cdot \mathbf{\Lambda}_i, \left\langle G^\Phi, \nabla' \cdot \mathbf{\Lambda} \right\rangle_{S_n} \right\rangle_{S_m} \tag{21}$$

$$V_i^m = -\left\langle \mathbf{\Lambda}_i, \mathbf{E}^a \right\rangle_{S_m}. \tag{22}$$

The double surface integrals are involved in the matrix element, which are evaluated by using a Gaussian quadrature when the two patches do not overlap. When they do, the method proposed by Duffy [29] is employed to evaluate the singular integrals. The applied field in the right-hand side is different for different problems. For scattering problems, the applied field is the electric field in the multilayer medium without microstrips. For circuit problems, a voltage delta source is usually applied to the excitation port so that the boundary edges on the excitation port are treated as unknowns.

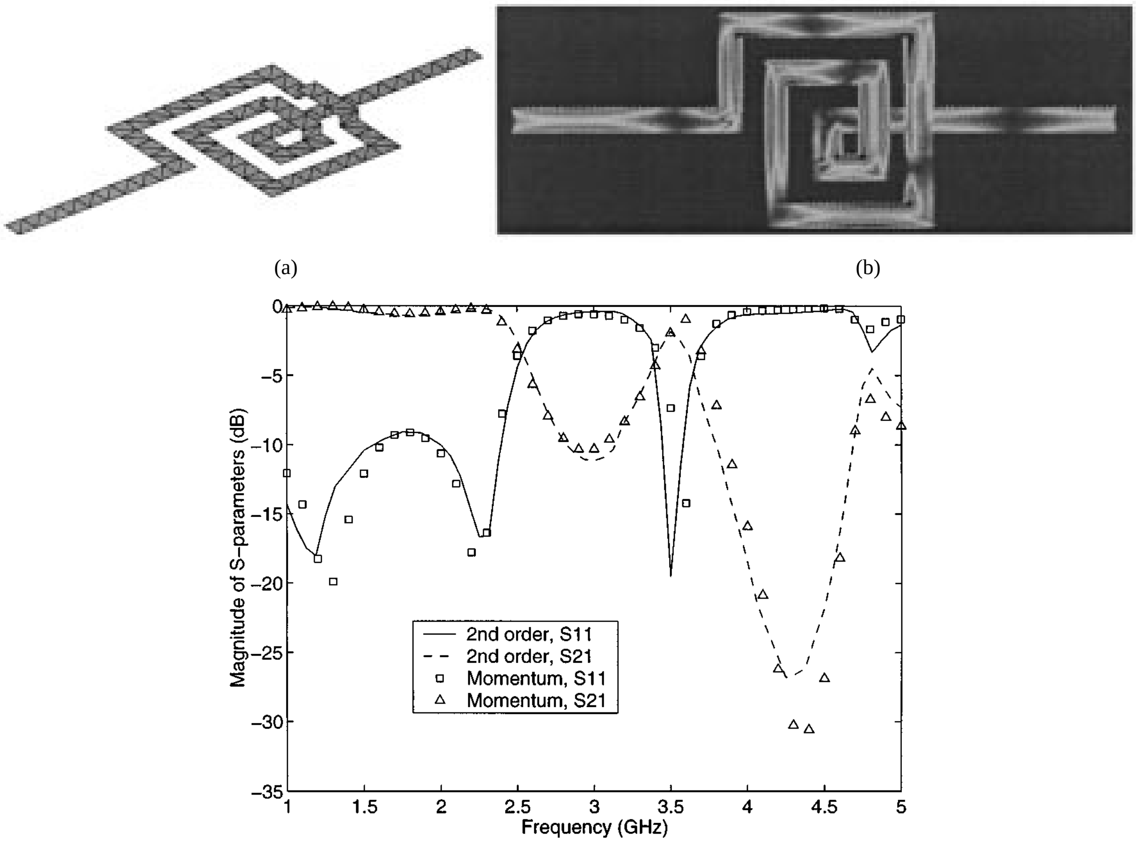

(c)

Fig. 8. S-parameters of a spiral inductor. The substrate has $\epsilon_r = 9.6$ and $h = 2.0$ mm. The linewidths and spacings are all 2.0 mm. The height and the span of the air bridges are 1.0 and 6.0 mm, respectively.

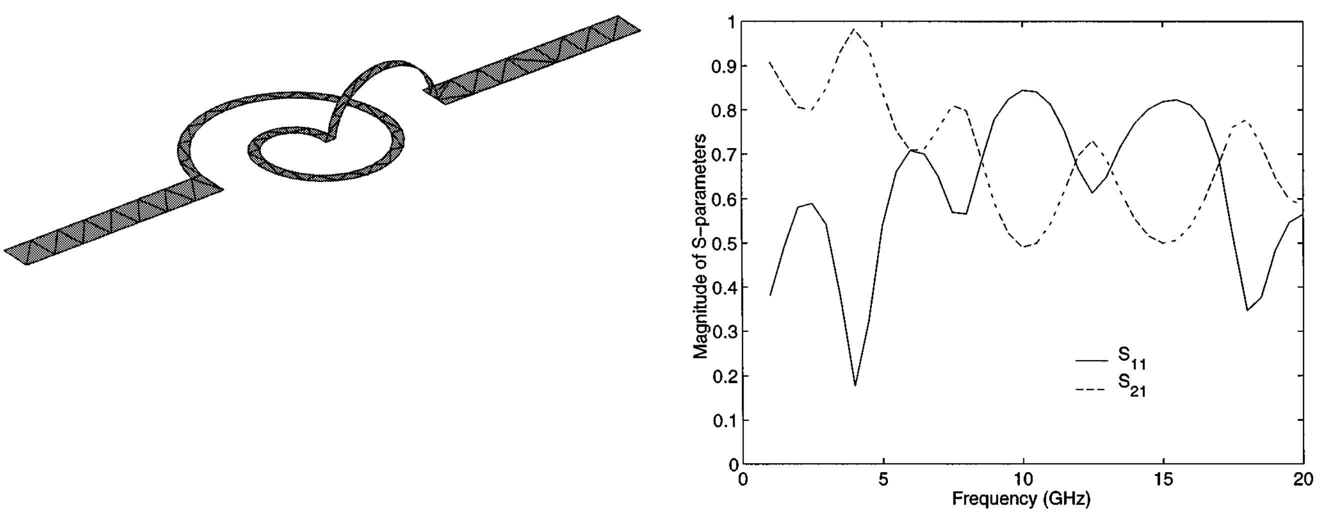

(a) (b)

Fig. 9. S-parameters of a spiral inductor. The substrate has $\epsilon_r = 9.8$ and $h = 0.635$ mm. See [33] for detailed information about the geometry.

Equation (20) can be solved to yield the current distribution on the microstrips. From the current distribution, radar cross sections for scattering problems, radiation patterns for antenna problems, or S-parameters for circuit problems can be determined [30]. For the S-parameter extraction, we use the three-point curve-fitting scheme together with the precalculated characteristic impedance and propagation constant of the corresponding microstrip line.

III. Numerical Results

To demonstrate the convergence behavior of higher order basis functions, we consider a circular microstrip patch, which has 1-cm radius and resides on a substrate with 2.2 relative permittivity and 0.787-mm thickness. The root mean square (rms) error in the monostatic radar cross section averaged over many angles of incidence at 10 GHz is calculated using the reference solution obtained by the third-order basis functions with an overly dense mesh. Fig. 6 shows the error and CPU time for matrix filling (excluding that for the initial Green's function generation, which is the same regardless of the order of basis function to be used). It is observed from this figure that, for the same number of unknowns, the higher order scheme gives more accurate results, and converges faster than the lower order scheme.

The second example is a four-port annular-ring power divider, which has been analyzed using an approximate planar circuit model that assumes a magnetic wall at the microstrip's edges [31]. Here, the curved boundaries are precisely modeled by curvilinear patches, as shown in Fig. 7. The results obtained using the second-order basis functions with 612 unknowns are given in Fig. 7. Also shown are the results computed using Momentum,[1] which uses zeroth-order basis functions with 1182 unknowns (The data of [31] is not shown here).

The examples above have no vertical currents so that only one component G_{xx}^A in $\bar{\mathbf{G}}^A$ is required to build the impedance matrix. In the following two examples, we show the capability of the method to deal with 3-D structures with both horizontal and vertical currents. The first example is a microstrip spiral inductors, which has previously been analyzed using the finite-difference time-domain (FDTD) method [32]. Its discretization is shown in Fig. 8(a), a top view of the current distribution at $f = 3.5$ GHz is displayed in Fig. 8(b), and the results obtained using the second-order basis functions with 1263 unknowns are given in Fig. 8(c). Also shown in Fig. 8(c) are the results computed using Momentum with 2247 unknowns, in which the vertical current is approximated by one rooftop basis function and the transverse current is neglected. These results also compare reasonably well with the FDTD solution in [32].

The second example is also an inductor, whose detailed geometrical information is given in [33]. The only difference here is that the bonding edge of the bridge and spire is shifted from the center to the side. The S-parameters calculated using the second-order basis functions with 840 unknowns are given in Fig. 9 along with the discretization of the structure.

IV. Conclusion

A MoM solution has been presented for the analysis of multilayer microstrip antennas and circuits. The required multilayer Green's functions have been evaluated by the DCIM, with the guided-mode contributions extracted recursively using a multilevel contour integral in the complex k_ρ-plane. An interpolation scheme has been employed to further speed up the calculation of the Green's functions in the 3-D space. Higher order interpolatory basis functions defined on curvilinear triangular patches have been used to provide necessary flexibility and accuracy to discretize arbitrary shapes and represent the electric currents on their surfaces. These higher order functions also offered a better convergence than the lower order ones. The combination of the DCIM with the guided-mode extraction and the higher order basis functions on curvilinear patches resulted in an efficient and accurate MoM analysis for 3-D multilayer microstrip structures.

[1] *Advanced Design System 1.5*, Agilent Technol., Palo Alto, CA, 2001.

References

[1] J. R. Mosig, "Integral equation techniques," in *Numerical Techniques for Microwave and Millimeter-Wave Passive Structures*, T. Itoh, Ed. New York: Wiley, 1988.

[2] J. Zhao, S. Kapur, D. E. Long, and W. W.-M. Dai, "Efficient three-dimensional extraction based on static and full-wave layered Green's functions," in *Proc. 35th Des. Automat. Conf.*, June 1998, pp. 224–229.

[3] R. C. Hsieh and J. T. Kuo, "Fast full-wave analysis of planar microstrip circuit elements in stratified media," *IEEE Trans. Microwave Theory Tech.*, vol. 46, pp. 1291–1297, Sept. 1998.

[4] T. J. Cui and W. C. Chew, "Fast evaluation of Sommerfeld integrals for EM scattering and radiation by three-dimensional buried objects," *IEEE Geosci. Remote Sensing*, vol. 37, pp. 887–900, Mar. 1999.

[5] W. Cai and T. Yu, "Fast calculations of dyadic Green's functions for electromagnetic scattering in a multilayer medium," *J. Comput. Phys.*, submitted for publication.

[6] D. G. Fang, J. J. Yang, and G. Y. Delisle, "Discrete image theory for horizontal electric dipole in a multilayer medium," *Proc. Inst. Elect. Eng.*, pt. H, vol. 135, pp. 297–303, Oct. 1988.

[7] Y. L. Chow, J. J. Yang, D. G. Fang, and G. E. Howard, "A closed-form spatial Green's function for the thick microstrip substrate," *IEEE Trans. Microwave Theory Tech.*, vol. 39, pp. 588–592, Mar. 1991.

[8] J. J. Yang, Y. L. Chow, G. E. Howard, and D. G. Fang, "Complex images of an electric dipole in homogeneous and layered dielectrics between two ground planes," *IEEE Trans. Microwave Theory Tech.*, vol. 40, pp. 595–600, Mar. 1992.

[9] R. A. Kipp and C. H. Chan, "Complex image method for sources in bounded regions of multilayer structures," *IEEE Trans. Microwave Theory Tech.*, vol. 42, pp. 860–865, May 1994.

[10] J. Van Hese, H. Rogier, K. Blomme, and N. Fache, "Calculation of spatial Green's functions: Numerical integration of Sommerfeld integrals versus complex image technique," in *Proc. Progress Electromag. Res. Symp.*, July 1994, p. 299.

[11] G. Dural and M. I. Aksun, "Closed-form Green's functions for general sources and stratified media," *IEEE Trans. Microwave Theory Tech.*, vol. 43, pp. 1545–1552, July 1995.

[12] M. I. Aksun, "A robust approach for the derivation of closed-form Green's functions," *IEEE Trans. Microwave Theory Tech.*, vol. 44, pp. 651–658, May 1996.

[13] C. H. Chan and R. A. Kipp, "Application of the complex image method to multilevel, multiconductor microstrip lines," *Int. J. Microwave Millimeter-Wave Computer-Aided Eng.*, vol. 7, pp. 359–367, 1997.

[14] ——, "Application of the complex image method to characterization of microstrip vias," *Int. J. Microwave Millimeter-Wave Computer-Aided Eng.*, vol. 7, pp. 368–379, 1997.

[15] F. Ling and J. M. Jin, "Discrete complex image method for general multilayer media," *IEEE Microwave Guided Wave Lett.*, vol. 10, pp. 400–402, Oct. 2000.

[16] B. Hu and W. C. Chew, "Fast inhomogeneous plane wave algorithm for electromagnetic solutions in layered medium structures—2D case," *Radio Sci.*, vol. 35, no. 1, pp. 31–43, Jan.–Feb. 2000.

[17] S. M. Rao, D. R. Wilton, and A. W. Glisson, "Electromagnetic scattering by surface of arbitrary shape," *IEEE Trans. Antennas Propagat.*, vol. AP-30, pp. 409–418, May 1982.

[18] J. C. Nedelec, "Mixed finite elements in R^3," *Numer. Math.*, vol. 35, pp. 315–341, 1980.

[19] R. D. Graglia, D. R. Wilton, and A. F. Peterson, "Higher order interpolatory vector bases for computational electromagnetics," *IEEE Trans. Antennas Propagat.*, vol. 45, pp. 329–342, Mar. 1997.

[20] J. P. Webb, "Hierarchal vector basis functions of arbitrary order for triangular and tetrahedral finite element," *IEEE Trans. Antennas Propagat.*, vol. 47, pp. 1244–1253, Aug. 1999.

[21] K. A. Michalski and D. Zheng, "Electromagnetic scattering and radiation by surfaces of arbitrary shape in layered media: Part I—Theory," *IEEE Trans. Antennas Propagat.*, vol. 38, pp. 335–344, Mar. 1990.

[22] K. A. Michalski and J. R. Mosig, "Multilayered media Green's functions in integral equation formulations," *IEEE Trans. Antennas Propagat.*, vol. 45, pp. 508–519, Mar. 1997.

[23] W. C. Chew, *Waves and Fields in Inhomogeneous Media*. Piscataway, NJ: IEEE Press, 1995.

[24] Y. Hua and T. K. Sarkar, "Generalized pencil-of-function method for extracting poles of an EM system from its transient response," *IEEE Trans. Antennas Propagat.*, vol. 37, pp. 229–234, Feb. 1989.

[25] D. C. Chang and J. X. Zhang, "Electromagnetic modeling of passive circuit elements in MMIC," *IEEE Trans. Microwave Theory Tech.*, vol. 40, pp. 1741–1747, Sept. 1992.

[26] F. Alonso-Monferrer, A. A. Kishk, and A. W. Glisson, "Green's functions analysis of planar circuits in a two-layer grounded medium," *IEEE Trans. Antennas Propagat.*, vol. 40, pp. 690–696, June 1992.

[27] M. J. Tsai, F. D. Flaviis, O. Fordham, and N. G. Alexopoulos, "Modeling planar arbitrarily shaped microstrip elements in multilayered media," *IEEE Trans. Microwave Theory Tech.*, vol. 45, pp. 330–337, Mar. 1997.

[28] W. H. Press, S. A. Teukolsky, W. T. Vettering, and B. P. Flannery, *Numerical Recipes in Fortran*, Cambridge, U.K.: Cambridge Univ. Press, 1992.

[29] M. G. Duffy, "Quadrature over a pyramid or cube of integrands with a singularity at a vertex," *J. Numer. Anal.*, vol. 19, pp. 1260–1262, Dec. 1982.

[30] F. Ling, C. F. Wang, and J. M. Jin, "An efficient algorithm for analyzing large-scale microstrip structures using adaptive integral method combined with discrete complex image method," *IEEE Trans. Microwave Theory Tech.*, vol. 48, pp. 832–839, May 2000.

[31] F. Tefiku and E. Yamashita, "Improved analysis method for multiport microstrip annular-ring power divider," *IEEE Trans. Microwave Theory Tech.*, vol. 42, pp. 376–381, Mar. 1994.

[32] M. Fujii and W. J. R. Hoefer, "A three-dimensional Haar-wavelet-based multiresolution analysis similar to the FDTD method—Derivation and application," *IEEE Trans. Microwave Theory Tech.*, vol. 46, pp. 2463–2475, Dec. 1998.

[33] A. C. Polycarpou, P. A. Tirkas, and C. A. Balanis, "The finite-element method for modeling circuits and interconnects for electronic packaging," *IEEE Trans. Microwave Theory Tech.*, vol. 45, pp. 1868–1874, Oct. 1997.

Feng Ling (S'97–M'99) was born in Jiangsu, China, in 1971. He received the B.S. and M.S. degrees in electrical engineering from the Nanjing University of Science and Technology, Nanjing, China, in 1993 and 1996, respectively, and the Ph.D. degree in electrical engineering from the University of Illinois at Urbana-Champaign (UIUC), in 2000.

From 1996 to 2000, he was a Research Assistant with the Center for Computational Electromagnetics (CCEM), UIUC. He is currently a Senior Engineer/Scientist with the Semiconductor Products Sector, Motorola, Tempe, AZ. His research interests include electromagnetic modeling of microwave integrated circuits, microstrip antennas, integrated passive components and interconnects for RF applications, and fast algorithms for computational electromagnetics.

Dr. Ling is a member of Phi Kappa Phi. He was the recipient of the 1999 Y. T. Lo Outstanding Research Award presented by the Department of Electrical and Computer Engineering, UIUC.

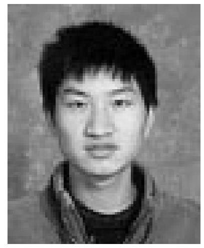

Jian Liu (S'00) received the B.S. and M.S. degrees in electrical engineering from the University of Science and Technology of China, Hefei, Anhui, China, in 1995 and 1998, respectively.

Since 1998, he has been with the Center of Computational Electromagnetics, University of Illinois at Urbana-Champaign, where he is currently a Research Assistant. His research interests include the application of finite-element and moment methods to electromagnetics problems.

Jian-Ming Jin (S'87–M'89–SM'94–F'01) received the B.S. and M.S. degrees in applied physics from Nanjing University, Nanjing, China, in 1982 and 1984, respectively, and the Ph.D. degree in electrical engineering from The University of Michigan at Ann Arbor, in 1989.

He is currently a Full Professor of electrical and computer engineering and Associate Director of the Center for Computational Electromagnetics, University of Illinois at Urbana-Champaign. His current research interests include computational electromagnetics, scattering and antenna analysis, electromagnetic compatibility, and magnetic resonance imaging. He has authored or co-authored over 110 papers in refereed journals and 15 book chapters. He has also authored *The Finite Element Method in Electromagnetics* (New York: Wiley, 1993) and *Electromagnetic Analysis and Design in Magnetic Resonance Imaging* (Boca Raton, FL: CRC Press, 1998), co-authored *Computation of Special Functions* (New York: Wiley, 1996), and co-edited *Fast and Efficient Algorithms in Computational Electromagnetics* (Norwood, MA: Artech House, 2001). His name is often listed in the University of Illinois at Urbana-Champaign's *List of Excellent Instructors*. He currently serves as an Associate Editor of *Radio Science* and is also on the Editorial Board for the *Electromagnetics Journal* and *Microwave and Optical Technology Letters*.

Dr. Jin is a member of Commission B of USNC/URSI, Tau Beta Pi, and the International Society for Magnetic Resonance in Medicine. He was an associate editor of the IEEE TRANSACTIONS ON ANTENNAS AND PROPAGATION (1996–1998). He was the symposium co-chairman and Technical Program chairman of the Annual Review of Progress in Applied Computational Electromagnetics in 1997 and 1998, respectively. He was a recipient of the 1994 National Science Foundation Young Investigator Award and the 1995 Office of Naval Research Young Investigator Award. He was also the recipient of the 1997 Xerox Junior Research Award and the 2000 Xerox Senior Research Award presented by the College of Engineering, University of Illinois at Urbana-Champaign. He was also appointed as the first Henry Magnuski Outstanding Young Scholar in the Department of Electrical and Computer Engineering, University of Illinois at Urbana-Champaign, in 1998. He was a Distinguished Visiting Professor with the Air Force Research Laboratory in 1999.